Meccanica (2016) 51:2797–2811
DOI 10.1007/s11012-016-0487-y

Experimental modal analysis of straight and curved slender beams by piezoelectric transducers

Gianfranco Piana · Egidio Lofrano · Alberto Carpinteri · Achille Paolone · Giuseppe Ruta

Received: 30 December 2015 / Accepted: 6 July 2016 / Published online: 18 July 2016

Abstract We present the use of piezoelectric disk buzzers, usual in stringed musical instruments to acquire sound as a voltage signal, for experimental modal analysis. These transducers helped in extracting natural frequencies and mode shapes of an aluminium beam and a steel arch in the laboratory. The results are compared with theoretical predictions and experimental values obtained by accelerometers and a laser displacement transducer. High accuracy, small dimensions, low weight, easy usage, and low cost, make piezoelectric pickups an attractive tool for the experimental modal analysis of engineering structures.

Keywords Experimental modal analysis · Piezoelectric sensors · Accelerometers · 1-D structures

1 Introduction

Experimental modal analysis is mostly based on measurements of displacement, velocity or acceleration, and excitation force [1–3]. This approach, sometimes referred to as Displacement Modal Testing (DMT), is well known in applied mechanics and engineering. Much literature on this subject exists, as papers in journals and congress proceedings on modal analysis, structural dynamics, and vibration. A different, not much diffused, approach based on strain measurements exists, referred to as Strain Modal Testing (SMT) [4–13], by which a direct measure of dynamic strain can be obtained, and stresses can be evaluated as well. Main cons of SMT are related to the practical use of strain gauges and sensors, with drawbacks strongly limiting its applicability (e.g., need of proper calibration, inadequate high frequency sensitivity, phase delay, amplitude loss, etc.). Recently, a novel miniaturized piezoelectric strain sensor, avoiding the main drawbacks of strain gauge measurements, has been tested for application in experimental modal analysis [14]. In this case, the main disadvantage is the cost of this piezoelectric strain sensor, which is presently rather high compared to that of standard mono-axial accelerometers.

In music technology piezoelectric pickups assure high quality recordings of stringed musical instruments (guitars, violins, etc.) since they convert mechanical vibration into an electrical signal. Piezoelectric disk beepers, or buzzers, have small size, low weight, wide frequency range, plus cost a few Euros: thus, they can be suitable for experimental modal analysis. Here we state their capabilities in this field on two simple one-dimensional specimens: a straight cantilever and a doubly hinged parabolic arch.

G. Piana · E. Lofrano · A. Paolone · G. Ruta (✉)
Dipartimento di Ingegneria Strutturale e Geotecnica, Università di Roma "La Sapienza", Rome, Italy
e-mail: giuseppe.ruta@uniroma1.it

A. Carpinteri
Dipartimento di Ingegneria Strutturale, Edile e Geotecnica, Politecnico di Torino, Turin, Italy

In this study, we tested the accuracy of piezoelectric disk buzzers in extracting the natural frequencies of both beam and arch: analytical predictions were the reference. We used 2 buzzers with different diameters, and a laser displacement transducer to make comparisons, for the cantilever. We evaluated the effect of self-weight on the fundamental frequency by means of both the piezoelectric pickup and the laser sensor. For the arch, only the smaller piezoelectric pickup was used, and placed at various locations to check if this affects the extraction of natural frequencies. The experimental results were compared with those previously obtained by some of the authors [15, 16], of finite element analyses and other experiments where mono-axial accelerometers were used. We then extracted mode shapes, by placing several piezoelectric pickups at the same time. The experimental results were compared to the analytical solution for the cantilever, and to those of finite element modelling and other experiments for the arch.

A preliminary study on the more general subject of dynamic identification was conducted, on the same benchmark cases, by some of the authors [17]. The aim of that contribution was limited to present the basics of the experimental apparatus and of the detecting devices and data acquisition system, plus some meaningful results. On the other hand, the present paper is intended to revise and complete the previous contribution: it contains new, unpublished results both on the cantilever beam and on the arch, based on new experimental campaigns, which were performed after the publication of [17].

For sake of completeness and convenience of reading, some general information about the experimental setting and data acquisition system are recalled here. At the same time, new formulas and more detailed explanations on both the experimental and numerical procedures adopted are added with respect to [17]. However, the results presented here on the modal curvatures and shapes of the cantilever beam are brand new, and are not the same with respect to the content of [17]. The following basic differences must be underlined: (1) the number of modes investigated was increased from 4 to 6; (2) the excitation points were changed; and (3) the exact expression of the curvature of a plane curve was used, instead of the linearised one adopted in [17], to obtain the mode shapes from the measured modal curvatures. More detailed comments are given in Sect. 3.2. In addition, all the results in the present paper about the modal curvatures and shapes of the arch are completely original: indeed, no result was available at the time when the contribution [17] was submitted for publication. As a matter of fact, the way to obtain the mode shapes of a curved structural element, like the considered arch, starting from curvature measurements provided by PZT pickups is a problem not trivial at all. Such a problem was not dealt with in [17], but, on the other hand, it represents an important part of the present paper.

2 Features and use of piezoelectric sensors

The adopted disk buzzers convert dynamic strain into an electric voltage signal (direct piezoelectric effect), thus they do not need any supply. The generated signal can be amplified if necessary, acquired by audio or usual acquisition devices, and therefore recorded and analyzed or manipulated. The sensors can be connected to the surface of the specimen simply by using glue or a thin film of gel, and their use does not require any calibration. Figure 1 shows a picture and a scheme of the type of sensors adopted in this study, while their main features are reported in Table 1. Two different diameters were selected for testing, i.e. 20 and 35 mm (sensors JPR-PLUSTONE 400-403 and 400-411, respectively).

3 Modal testing of an aluminium cantilever beam

3.1 Experimental setup

We tested an aluminium cantilever beam with rectangular cross section ($b \times t = 25 \times 1.97$ mm), clamp 100 mm long, and free length $L = 470$ mm. Young's modulus $E = 62$ GPa was given by static deflection measurements; the weight of the element yields mass per unit length $m = 0.128$ kgm^{-1} (material mass density $\rho = 2600$ kgm^{-3}). Figure 2 shows the setup for the evaluation of the natural frequencies: in Fig. 2a, a laser displacement transducer is placed at the beam tip; in Fig. 2b, a piezoelectric pickup is placed near the clamp (diameters 35 mm, left, 20 mm, right). The laser optoNCDT 1302-20 is a triangulating displacement sensor produced by Micro-Epsilon with 10 μm resolution for dynamic acquisitions at 750 Hz

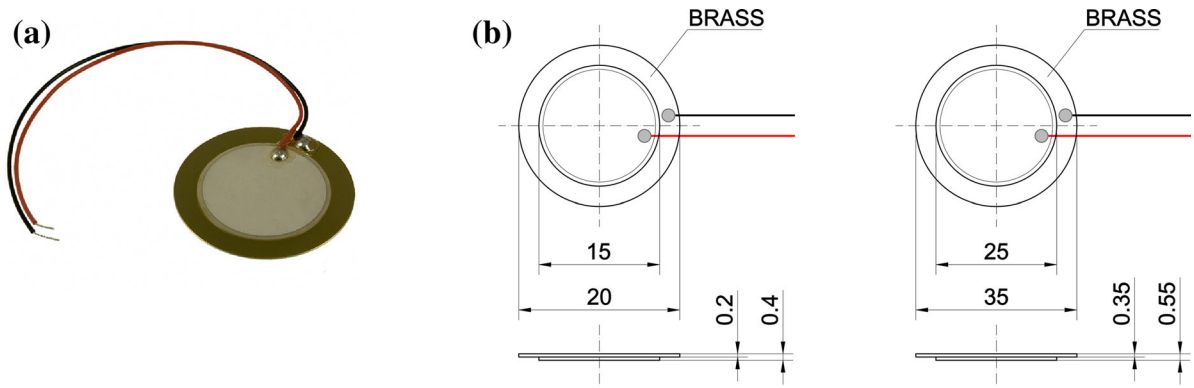

Fig. 1 **a** Photo and **b** schemes (dimensions in mm) of the adopted piezoelectric disk buzzers

Table 1 Main characteristics of the adopted piezoelectric sensors

Sensor	External diameter (mm)	Frequency range	Resonant frequency (kHz)	Operating temperature	Average weight (incl. wires) (g)
JPR-PLUSTONE 400-403	20	~0 to 20 kHz	6.0 ± 0.5	−20 to +50 °C	1.16
JPR-PLUSTONE 400-411	35		3.0 ± 0.5		3.60

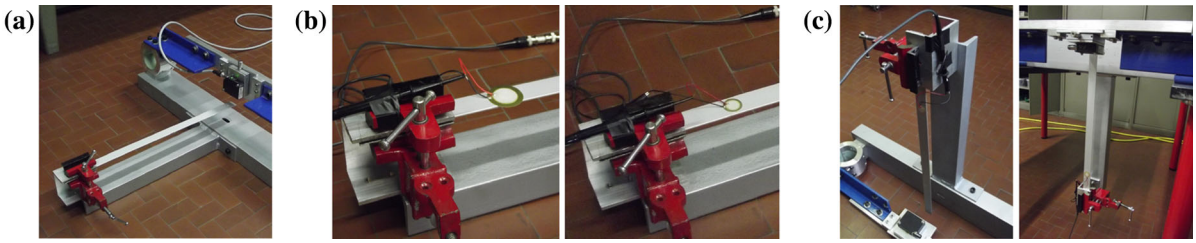

Fig. 2 Experimental setup for extracting the natural frequencies of a cantilever beam: **a** laser sensor and **b** piezoelectric pickups ($\phi = 35$ mm, *left*; $\phi = 20$ mm, *right*), **c** cantilever subjected to axial force due to self-weight (stretched, *left*; shortened, *right*)

top frequency, and 20 mm default measuring range. The operator can narrow this range to use the maximum resolution on a reduced distance range; midrange is placed 40 mm from the surface of the transducer. The piezoelectric pickups were connected to the specimen surface by a thin film of gel, and placed close to the clamp, where maximum strain occurs. This is a key difference with respect to DMT and, similar to SMT, piezoelectric disks shall better be placed where top strains occur. Conversely, in modal testing based on acceleration measures, accelerometers shall better be placed where top displacement occurs. Thus, bad locations are close to the nodes of modes for accelerometers, and to the points of null strain (e.g., a cantilever tip) for piezoelectric buzzers.

Figure 2c shows the setup to evaluate the variation of the fundamental frequency induced by self-weight, when the cantilever was stretched (left) or shortened (right). Signals from both laser sensor and disk buzzers were acquired without pre-amplification by a NI 9215 data acquisition device produced by National Instruments. This is a 4 channels-device, with 16 bits resolution, 100 kHz maximum sampling frequency, and −10 to 10 V operating voltage range. Acquisition, processing and post-processing of measured signals were made using LabVIEW software.

Figure 3 shows the experimental setup to extract mode shapes: 6 pickups were placed as in Fig. 3b, and only 20 mm diameter piezoelectric disks were used (Fig. 3a). An audio acquisition device Audiobox

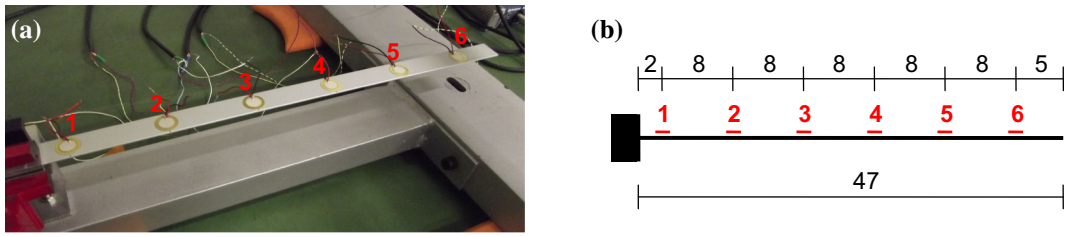

Fig. 3 Experimental setup for extracting modal curvatures and shapes of a cantilever beam: **a** picture and **b** locations of sensors (dimensions in cm)

1818VSl, produced by PreSonus, caught the signals generated by the pickups, and WAV (Waveform Audio File Format) files were obtained. The acquisition unit had 8 channels, allowing recording with 24 bits resolution at 44.1, 48.0, 88.2, and 96.0 kHz. We choose a 44.1 kHz sampling frequency for measurements, and processed and recorded the acquired signals by the sound recording software Studio One 2, produced by PreSonus; Matlab and Maple were used for post-processing.

3.2 Results and comparisons

Fourier analysis of the measured free response signals provided the natural frequencies; only the output was recorded, and Power Spectral Density (PSD) was used to detect the frequencies (computations were made using Matlab). For each sensor, six impulsive excitations were given to the beam to study the consequent free response. The excitation was represented by an impact force transmitted to random points of the specimen by means of a not-instrumented light impact hammer. Each evaluated frequency is the mean of six values. Table 2 provides comparisons of the mean natural frequencies provided by the disks with the corresponding analytical values [1]. The sampling frequency, 750 Hz, was the maximum for the laser sensor. We see the laser cannot catch the fourth frequency (241.90 Hz), while the two disks can. The percentage differences $(f_e - f_t)/f_t \times 100$ between the experimental and theoretical values f_e,f_t are always extremely small, see Table 2. Since piezoelectric disks have little mass compared to that of the specimen, although this is a relatively lightweight element, their output perfectly compares to that of a non-contact transducer like the laser sensor. Indeed, the sensor-to-specimen mass ratio is equal to 1.93 and 5.98 % for the smaller and the larger pickup, respectively. The smaller pickup provided a better output than the larger one, since its mass is lower. In addition, we observe that even if the diameter of the brass support of the latter (35 mm) exceeded the beam width (Fig. 2b), the diameter of the actual sensor (white part) is equal to 25 mm (Fig. 1b), and therefore exactly fits the specimen. Both pickups provide higher detection accuracy at lower frequencies, but this is related to the adopted sampling frequency and to the part of the analyzed signal, and is not a general conclusion. As far as the sampling frequency is concerned, theoretical considerations suggest adopting at least twice the value of the maximum frequency of interest as a sampling frequency (Nyquist criterion) [1, 2]. However, practical instructions suggest to multiply the maximum desired frequency by 10, thus providing in our case a recommended sampling frequency of 2400 Hz to investigate up to the fourth mode.

The first 6 natural frequencies extracted by the 20 mm pickup at 20 kHz sampling frequency are in Table 3: given the mean μ, small values of standard deviation σ and coefficient of variation $CV = \sigma/\mu$ denote a low dispersion of measures. Tables 2 and 3 show that increasing the sampling frequency improved the accuracy in detecting the 3rd and 4th frequencies, according to what we pointed out before. Conversely, the first frequency has a slightly less accurate value in Table 3 than in Table 2, since increasing the sampling frequency and setting the time window over the first part of the response to detect a larger number of frequencies affected negatively the accuracy in detecting the fundamental frequency.

As it is known, axial loads affect the bending rigidity of slender beams because of second-order effects. For a simply supported purely flexible elastic beam with uniform cross-section under a ‘dead’ axial load, the square of the natural

Table 2 Comparison of natural frequencies for the cantilever in Fig. 2a, b by laser and PZT sensors at 750 Hz sample frequency

Mode	Theoretical	Laser		PZT ($\phi = 35$ *mm*)		PZT ($\phi = 20$ *mm*)	
	f (Hz)	f (Hz)	Diff. (%)	f (Hz)	Diff. (%)	f (Hz)	Diff. (%)
1	7.03	7.00	−0.4	7.00	−0.4	7.00	−0.4
2	44.09	44.20	0.2	43.90	−0.4	44.02	−0.2
3	123.45	123.40	0.0	120.75	−2.2	122.17	−1.0
4	241.90	–	–	233.30	−3.7	239.48	−1.0

Table 3 Natural frequencies of the cantilever in Fig. 2b by PZT ($\phi = 20$ *mm*) at 20 kHz sampling frequency (mean values μ, standard deviations σ, and coefficients of variation *CV*)

Mode	μ (Hz)	σ (Hz)	*CV* (%)	Mode	μ (Hz)	σ (Hz)	*CV* (%)
1	7.11	0.38	5.34	6	596.43	0.63	0.11
2	43.76	0.51	1.17	7	829.03	0.91	0.11
3	123.29	0.25	0.20	8	1102.22	1.07	0.10
4	242.37	1.21	0.50	9	1418.85	2.06	0.15
5	396.94	0.49	0.12	10	1779.99	1.06	0.06

Table 4 Variation of the fundamental frequency of the cantilever beam in Fig. 2 induced by the axial load due to self-weight (positive p means tension)

Axial load due to self weight	Theoretical		Laser		PZT ($\phi = 35$ *mm*)		PZT ($\phi = 20$ *mm*)	
	f_1 (Hz)	Variat. (%)	f_1 (Hz)	Variat. (%)	f_1 (Hz)	Variat. (%)	f_1 (Hz)	Variat. (%)
$p = 0$	7.03	–	7.02	–	7.03	–	7.01	–
$p = 1.26$ N/m	7.09	0.85	7.08	0.85	7.08	0.71	7.08	0.99
$p = -1.26$ N/m	6.98	−0.72	6.97	−0.72	6.97	−0.86	6.96	−0.72

frequencies is linear with the load [18–22]. In particular, in case of compression the n-th bending frequency decreases from the value corresponding to the eigenvibration of the unloaded beam down to zero when the n-th buckling load is reached; indeed, the vanishing of an eigenfrequency corresponds to a static loss of stability (i.e., buckling), according to the dynamic criterion [23]. Each frequency-load path never crosses the others. Conversely, tensile loads imply the opposite behaviour, i.e., the eigenfrequencies increase with the applied force; in this case, frequency crossing may occur. In general, except for a few cases, for other constraint or loading conditions the relationships between the square of the eigenfrequencies and the applied axial load are no longer linear; this is because, in general, the axial load modifies the mode shapes. However, in most cases this effect on mode shapes is almost negligible, and the frequency squared vs. axial load relation is only slightly non-linear [22]. Thus, the linear approximation can usually be adopted in most cases with a small error. For simply supported conditions and uniform axial load, the mode shapes (sine waves) are not affected at all [24].

We checked the capability of the pickups to detect the variation of the first frequency in vertical beams due to self-weight: indeed, the fundamental frequency increases (decreases) when the beam is vertical with tip downwards (upwards). Self-weight induces a uniformly distributed axial load $p = \pm\ 1.26\ \mathrm{Nm}^{-1}$ (positive if tensile, negative otherwise): such a low magnitude implies a very small variation of the first frequency, the square of which is approximately linear in the distributed axial load [22]:

$$\left(f_1/f_{1,0}\right)^2 = 1 + \left(p/|p_{cr}|\right) \quad (1)$$

with $f_{1,0}$ the first frequency of the unloaded cantilever (i.e.,$p = 0$) and p_{cr} the buckling load [22]:

$$p_{cr} \approx -7.837 EIL^{-3} \approx -74.54 \text{ Nm}^{-1} \quad (2)$$

with EI the bending stiffness. Table 4 compares experimental results and theoretical values; self-weight induces a percentage variation $[f_1 (p = \pm 1.26) - f_1 (p = 0)]/f_1 (p = 0) \times 100$ in the first frequency. The results show that both piezoelectric disks could detect the small variation in the fundamental frequency induced by self-weight, with a precision comparable to that of a non-contact transducer, like the adopted laser sensor. Remark that in this case the fundamental frequency is detected with higher accuracy than that in Tables 2 and 3. In this case the excitation was not represented by an impulsive force. Indeed, in order to excite mainly the first mode, we slightly bent the cantilever by imposing a displacement at the tip; then the beam was released, with no initial velocity, and the free decay of the response registered. We thus obtained the experimental values in Table 4 by the Logarithmic Decrement Method [1, 2] applied to the final part of the signal, where the first frequency prevails. Each result represents the mean of six values. In Table 4, the maximum percentage difference between experimental and theoretical values equals −0.29 % (i.e., (6.96 − 6.98)/6.98 × 100) and in one case the results actually coincide. Unlike the case of the beam in horizontal position, in this case the larger pickup worked better than the smaller one in two out of three cases, while in the other they produced the same result (Table 4).

We extracted the mode shapes by the setup shown in Fig. 3; only 20 mm diameter pickups were used. Three impulsive forces (impact) were transmitted at each sensor (on the opposite face of the specimen) by means of a not-instrumented light impact hammer; six free response signals were obtained for each excitation (6 pickups), which multiplied for a total of 18 excitations yields a overall number of recorded signals equal to 108. The Peak Picking Method was used [1–3]. By the piezoelectric pickup we measure a voltage signal that is proportional to the average strain in the surface where the contact between the sensor and the specimen occurs. We assume, as it is usual in beams, that cross-sections remain plane during the deformation of the specimen. Then, once given the depth of the cross-section, a good estimate of the curvature is possible by means of a simple linearity relationship between curvature and longitudinal strain. Therefore, the first six modal curvatures were directly detected as follows: (1) the Fast Fourier Transform (FFT) of each acquired response signal was computed; (2) their imaginary parts were extracted for each applied impulse at the identified natural frequencies, so to build receptance-like matrices [1–3], and thus evaluate the modal curvatures at each sensor; (3) for each mode, curvature values from different measurements were suitably normalized and averaged to obtain a single curvature value at each sensor (null values were added at the cantilever tip, where no strain is, thus obtaining $N + 1$ values, with $N = 6$ the number of sensors); and (4) for each mode, the curvature values $\kappa(z_j)$, $j = 1,2,\ldots,N + 1$, were interpolated via cubic splines [25] to yield the modal curvature $\kappa(z)$ on the interval [$z_1 = 2$ cm, $z_7 = L$= 47 cm], and therefore on the whole domain $z \in [0, L]$ by extrapolation. When interpolating with cubic splines, the curvature $\kappa(z)$ is described by N piecewise cubic polynomials which are continuous with continuous derivatives up to order 2 on the N intervals between sensor 1 and the tip. Intervals may have different width (i.e., points may be unequally spaced). The requirement that $\kappa(z)$ is continuous and goes through the $N + 1$ points results in two conditions on each interval; the requirement that the first and the second derivatives of $\kappa(z)$ are continuous results in two additional conditions on each interval. All the previous requirements therefore introduce an overall number of $4N - 2$ constraint conditions. Since we have N polynomials and each polynomial has 4 free coefficients, there are a total of $4N$ unknown coefficients. With $4N - 2$ constraints and $4N$ unknowns, two more conditions are required for a unique solution. These conditions are usually chosen to be end conditions on $\kappa(z)$ or its derivatives. However, instead of solving a linear system of order $4N$, an opportune choice of the two additional conditions allows solving a linear system of order at most $N + 1$. In any case, the sought spline exists and is unique. The generic cubic spline associated to nodes z_j (supposed fixed) depends on $N + 3$ parameters: the $N + 1$ ordinated $\kappa(z_j)$ and the two additional conditions at the ends [25]. Maple was used for interpolation; input requires vectors containing the abscissas z_j and the ordinates $\kappa(z_j)$ of the

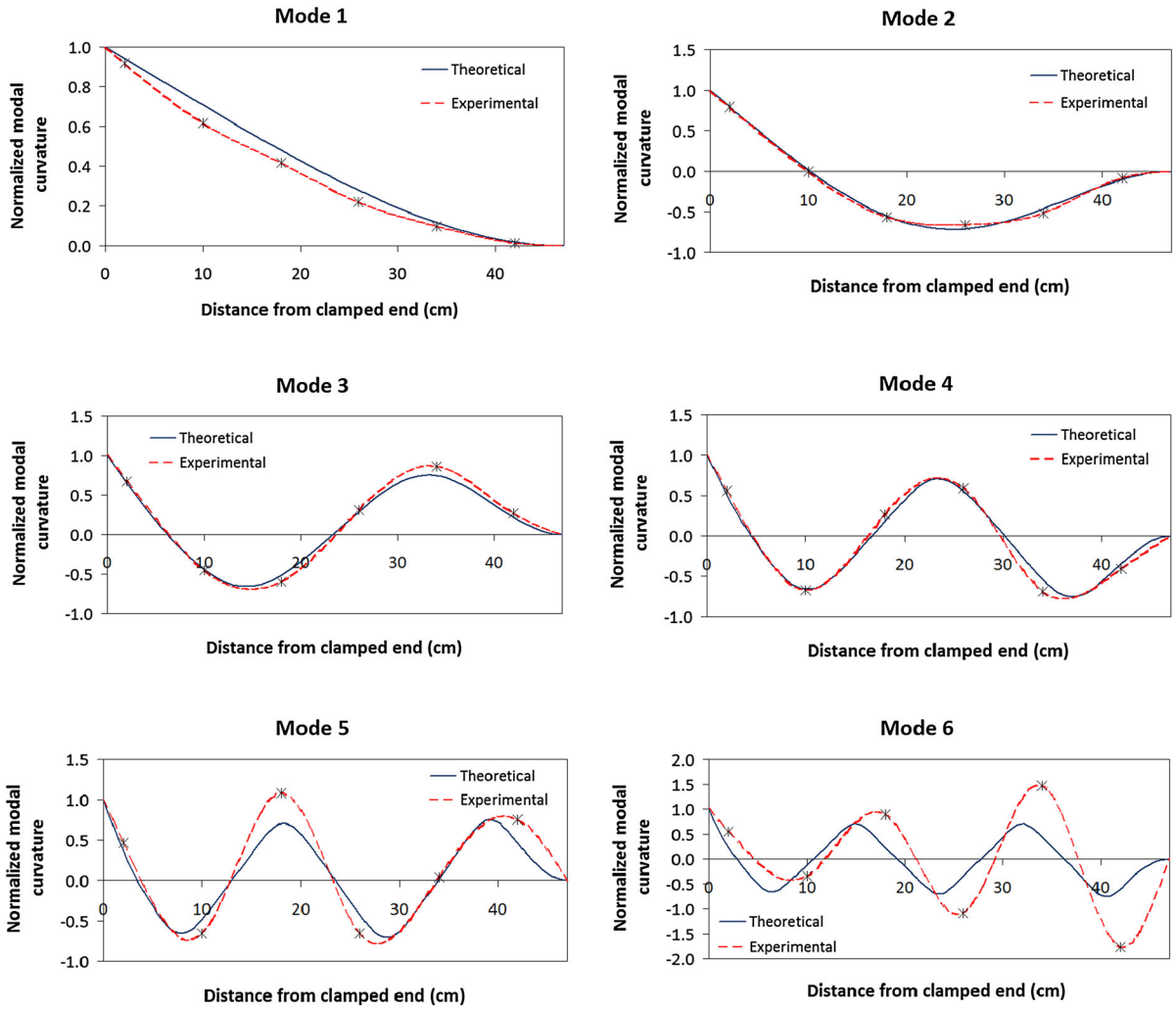

Fig. 4 First six normalized modal curvatures for the cantilever beam in Fig. 3

points to be interpolated, plus the desired order of the splines (here, 3). Once modal curvatures are found, a numerical integration along the abscissa, plus relevant boundary conditions, yields the mode shapes. The exact expression of the curvature $\kappa(z)$

$$\kappa(z) = \frac{\mathrm{d}^2 y(z)}{\mathrm{d}z^2}\left[1 + \left(\frac{\mathrm{d}^2 y(z)}{\mathrm{d}z^2}\right)^2\right]^{-3/2} \tag{3}$$

of a plane curve $y(z)$, $z \in [0, L]$, was used for integration. In detail, the curvatures $\kappa_i(z)$, $i = 1,2,\ldots,6$, were known for each i-th mode, while the mode shape functions $y_i(z)$ had to be determined solving Eq. (3) with the boundary conditions $y(0) = y'(0) = 0$ (prime denotes derivative with respect to z). Maple was used to solve Eq. (3). Lastly, the modal curvatures and shapes were normalized with respect to the values at clamp and tip, respectively.

Figures 4 and 5 show comparisons among experimental and theoretical results in terms of mode curvatures and shapes, respectively. Figure 4 shows that the pickups catch modal curvatures with high precision. Figure 5 shows that the results are good also in terms of mode shapes, with the only exception of modes 5 and 6, for which the results are unsatisfactory; for the first two mode shapes, in particular, the experimental and theoretical curves are practically superposed, and it is almost the same for the third mode.

We evaluated the correlation among experimental and theoretical results for mode curvatures and shapes by the Modal Assurance Criterion (*MAC*) [26] and the Normalized Modal Difference (*NMD*) [27]. *MAC* is probably the most common procedure to correlate two sets of mode vectors and is defined as:

$$MAC\left(\phi_{A,k},\phi_{B,j}\right)=\frac{\left(\phi_{A,k}^{T},\phi_{B,j}\right)^{2}}{\left(\phi_{A,k}^{T},\phi_{A,k}\right)\left(\phi_{B,j}^{T},\phi_{B,j}\right)}, \tag{4}$$

with $\phi_{A,k}$ the k-th mode of the data set A and $\phi_{B,j}$ the j-th mode of the data set B. *MAC* is analogous to the correlation coefficient in statistics and is unaffected by the individual scaling of mode vectors. *MAC* ranges [0, 1]: 1 implies perfect correlation of the two mode vectors, while 0 indicates uncorrelated, or orthogonal, vectors. Usually, $MAC > 0.80$ implies a good match, while $MAC < 0.40$ yields a poor match. *NMD* is related to *MAC* by

$$NMD\left(\phi_{A,k}\phi_{B,j}\right)\sqrt{\frac{1-MAC\left(\phi_{A,k}\phi_{B,j}\right)}{MAC\left(\phi_{A,k}\phi_{B,j}\right)}} \tag{5}$$

In practice, *NMD* is a close estimate of the average difference between the components of the vectors, $\phi_{A,k}$, $\phi_{B,j}$; e.g., if *MAC* equals 0.950, then *NMD* is 0.2294, meaning that the components of $\phi_{A,k}$ and $\phi_{B,j}$ differ 22.94 % average. *NMD* is much more sensitive to mode shape differences than the *MAC* and hence is introduced to highlight the differences between highly correlated mode shapes.

We carried out the correlation analysis considering the lists of curvatures and vertical displacements at the instrumented sections as vectors, for modal curvatures and mode shapes respectively. Results are in Table 5 and show a very high correlation between experimental and analytical modal curvatures for all modes 1 to 6. The first three mode shapes have also good correlation, but it is not so for the fourth one. On the other hand, the 5th and 6th experimental and analytical mode shapes are almost uncorrelated (bold-face in Table 5). Such a discrepancy shall be imputed to an error amplification by the interpolation-integration procedure for higher modes. Indeed, although the 5 and 6th experimental and numerical modal curvatures have excellent correlation (see Table 5), interpolation and then integration along z led to a quite poor match of experimental and numerical mode shapes (see Fig. 4). Thus, increasing the number of sensors can control and reduce the error in reconstructing higher mode shapes. Anyway, the re-construction of modal curvatures is quite good. Even though in general, as a principle, six sensors should be sufficient to detect as many modal curvatures (the curvature value at the tip is known to be zero), in practice it is always advisable to use a number of sensors larger than the desired number of modes.

The results obtained in the present work for modal curvatures and shapes are better than the corresponding ones obtained in our preliminary study [17]. In that case, the first four modal curvatures were detected by transmitting three impulsive forces to the midpoint between sensors 1–2, 2–3, 3–4, 4–5, 5–6, and between sensor 6 and the tip of the cantilever; however, in the present case we excited in correspondence to each sensor, thus constructing the receptance-like matrices more correctly. Furthermore, in [17] we obtained the mode shapes from the measured curvatures by means of the linearised expression of the curvature $\kappa(z) = \mathrm{d}^2y/\mathrm{d}z^2$ instead of the exact expression (3) adopted here. A comparison in terms of *MAC* and *NMD* values between the present study and the previous one [17] shows that: (1) the modal curvatures were detected with more accuracy by the present investigation, although in both cases the estimate was very good; (2) in [17] only the first three mode shapes were correctly detected, with very good result limited to modes 1 and 3; conversely, in the present work the results are not bed up to the fourth mode, with an very good estimate of the first three mode shapes.

4 Modal testing of a steel doubly hinged parabolic arch

4.1 Experimental setup

The specimen, Fig. 6a, is a doubly hinged parabolic steel arch like that used in [28] for dynamic damage identification, with span $L = 1010$ mm, rise $F = 205$ mm (rise-to-span ratio $F/L = 0.203$), rectangular cross-section ($b \times t = 40 \times 8$ mm), Young's modulus $E = 205$ GPa, Poisson's ratio $\nu = 0.3$, and mass density $\rho = 7849$ kgm^{-3} (mass per unit length $m = 2.512$ kgm^{-1}). Red circles in Fig. 6a indicate the instrumented sections.

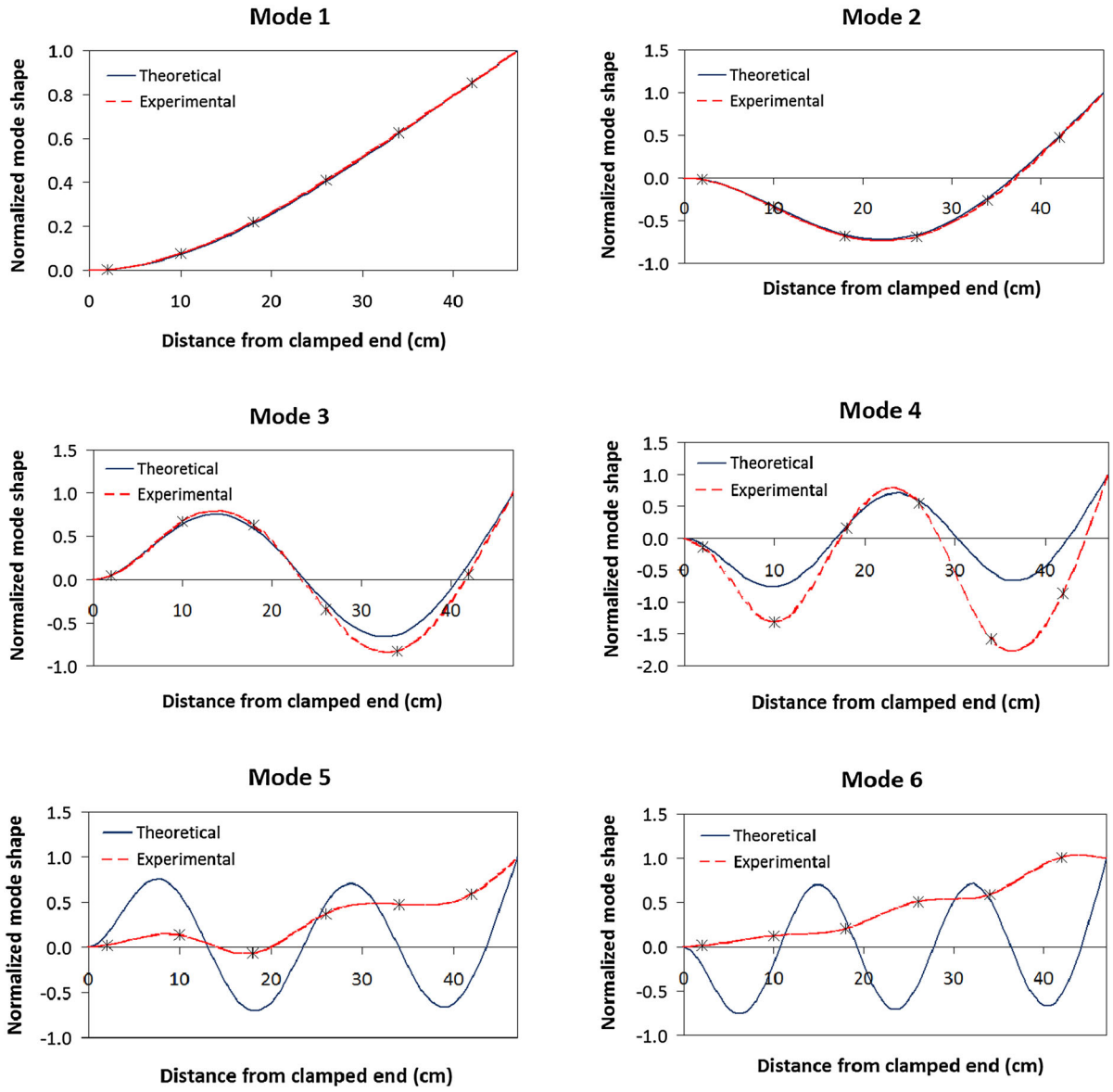

Fig. 5 First six normalized mode shapes for the cantilever beam in Fig. 3

We used only 20 mm piezoelectric disks in the tests, with setup in Fig. 6b. A single pickup, placed at the Sections 4, 5, 6, and 7 of Fig. 6a alternatively in order to check the best location, was used to extract natural frequencies first. The signals were pre-amplified by a differential amplifier, and then acquired by a NI 9215 data acquisition device by National Instruments. LabVIEW was used for acquisition, processing and post-processing operations. Subsequently, seven pickups were placed at one time at Sections 1–7 of Fig. 6a to extract modal curvatures and shapes, as shown also in the enlarged Fig. 7. As for the cantilever, we used the Audiobox 1818VSl and the software Studio One 2 by PreSonus to acquire and process signals, while post-processing was done using Matlab and Maple. Lastly, Fig. 6c shows the setup of a previous study [15], where seven uniaxial piezoelectric accelerometers were placed at Sections 1–7 of Fig. 6a.

Table 5 *MAC* and *NMD* values for modal curvatures and mode shapes shown in Figs. 4 and 5

	Modal curvatures		Mode shapes	
Mode	*MAC*	*NMD*	*MAC*	*NMD*
1	0.9898	0.0935	0.9999	0.0091
2	0.9931	0.0781	0.9670	0.1425
3	0.9925	0.0729	0.9665	0.1668
4	0.9858	0.1098	0.7038	0.6829
5	0.9920	0.0850	**0.0167**	**11.4985**
6	0.9890	0.1045	**0.1047**	**2.9399**

4.2 Results and comparisons

The first six natural frequencies of in-plane vibration were extracted by the same procedure used for the cantilever, i.e., Fourier analysis of free response signals with 3 kHz sampling frequency. The arch was excited by five external impulses for each point, transmitted at positions 1, 2, midpoint between 2 and 3, and 4 (Fig. 6a); a total of 20 signals were registered and analyzed. The excitation points are the same as in [15]. The impulsive forces were transmitted by a non-instrumented impact hammer; therefore, only the

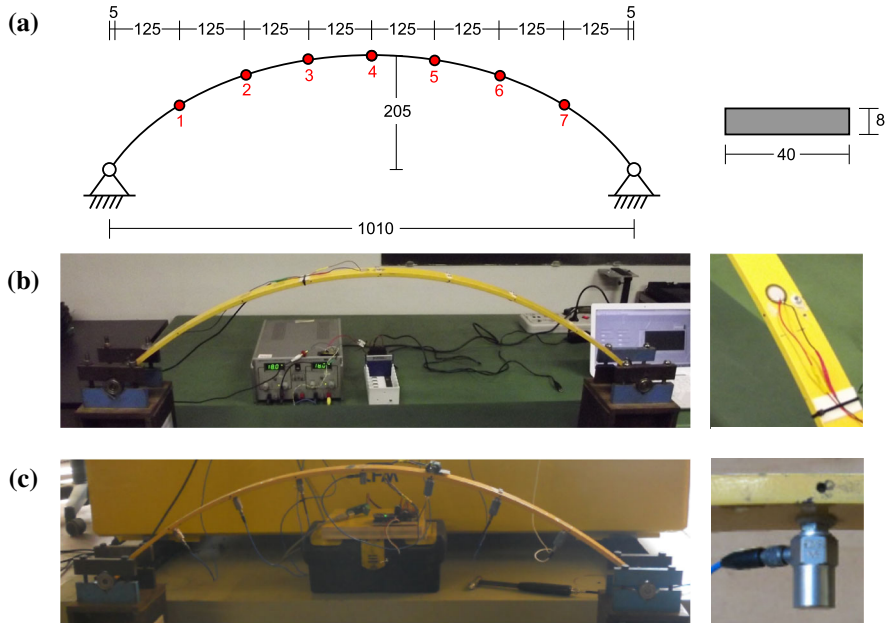

Fig. 6 Experimental setup for the steel parabolic arch: **a** dimensions in mm (*red circles* indicate the instrumented sections), **b** test with piezoelectric pickups, **c** test with accelerometers [15]. (Color figure online)

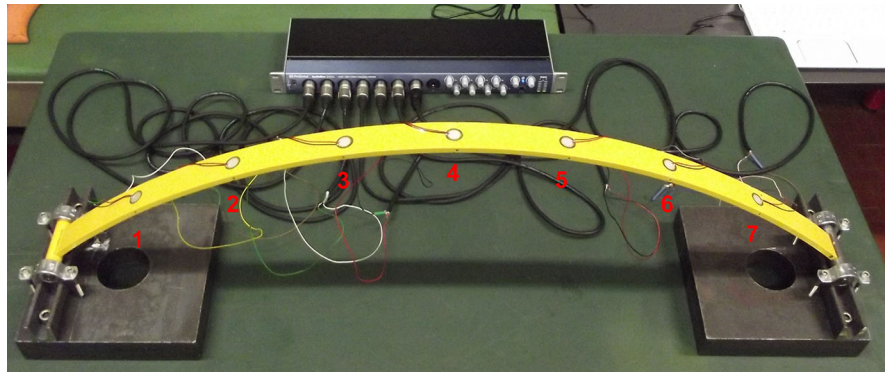

Fig. 7 Experimental setup for extracting modal curvatures of the parabolic arch by piezoelectric pickups

output was registered, as for the cantilever. Table 6 reports the statistics for the identified frequencies: mean values μ, standard deviations σ, and coefficients of variation CV. The values of σ and CV denote the low dispersion and reliability of all data. In general, the best locations of sensors for the extraction of many natural frequencies correspond to places 6 and 7 of Fig. 6a; for instance, as it could have been expected, frequencies corresponding to odd modes were detected with less accuracy when the sensor was located at midpoint, position 4 of Fig. 6a.

Finite element models were implemented to evaluate the frequencies of interest by a linear dynamic eigenvalue analysis. They were built by modelling the arch centreline by curved Timoshenko-like beam elements; when accelerometers were used, the additional masses were taken into account. A comparison of experimental and numerical frequencies is in Table 7 for both the present campaign (piezoelectric disk) and a previous one (accelerometers) [15]. The percentage differences $(f_n - f_e)/f_e \times 100$, f_n and f_e being the numerical and experimental frequencies respectively, are reported in Table 7. A good agreement between numerical and experimental results is apparent for all the identified frequencies. Remark, however, that the frequencies provided by the accelerometers are lower than those identified by piezoelectric disks, because of the additional masses of accelerometers and cables, the values of which are not negligible with respect to the arch mass (this effect was considered in [15]). As a general comment, piezoelectric pickups allow for a precise extraction of the resonant frequencies also for a curved structural element such as the parabolic arch; moreover, while the precisions of pickups and accelerometers appear comparable, the mass of the former is so small that the mass of the specimen is practically not perturbed.

Table 6 Identified natural frequencies of the arch: mean values μ, standard deviations σ, and coefficients of variation CV

Mode	μ (Hz)	σ (Hz)	CV (%)
1	54.6	0.49	0.89
2	127.0	1.06	0.84
3	231.1	0.76	0.33
4	360.0	0.70	0.19
5	521.4	0.90	0.17
6	721.7	0.84	0.12

We extracted modal curvatures and shapes by the setup shown in Fig. 7. Five impulsive excitations were transmitted in correspondence to each of the seven sensors (on the opposite face of the arch) by an impact hammer, and the audio box recorded the response signals, with a sampling frequency of 44.1 Hz and a resolution of 24 bits; a total of 245 signals were registered and analysed. The first six modal curvatures were then extracted by a procedure analogous to that described for the cantilever. Once the modal curvatures are determined, by modelling the specimen as a Kirchhoff arch (i.e., an inextensible and shear non-deformable curved beam, which is reasonable for the analyzed geometry), the mode shapes can be directly obtained via a numerical integration with respect to the arc length (plus the relevant boundary conditions). Indeed, in this case the exact expressions of the tangential and transversal displacement fields u, v are related to the mechanical and initial (geometrical) curvatures κ, k through

$$\begin{aligned} u''(s(z)) &= [k(s(z))v(s(z))]', \\ v''(s(z)) &= -[k(s(z))u(s(z))]' + \kappa(z) \end{aligned} \tag{6}$$

where the arch length s is in terms of the abscissa z. Since we know k, κ, the analytical or numerical solution of the second-order ODEs (6) directly provides u, v. We normalize modal curvatures with respect to their maximum value, and mode shapes with respect to a maximum transverse displacement of a quarter raise, to improve graphic representation.

Figures 8 and 9 show the comparisons among the experimental results obtained by the pickups and their numerical counterparts, in terms of modal curvatures and shapes, respectively. Figure 10 shows a comparison among the experimental mode shapes provided by the accelerometers and the relevant numerical shapes obtained by taking the accelerometers masses into account. To this aim, the signals recorded during the experimental campaign described in [15, 16] have been analyzed here by the same procedure described for the strain measurements. Remark that, since the pickup number 5 (see Fig. 7) gave results quite far from the expected values (probably because of a failure in the sensor or in the acquisition system), the relevant curvatures were replaced by exploiting the symmetry of the problem, that is, using the value of the sensor 3 for even modes, and its opposite for odd ones.

Table 7 Comparison among experimental and numerical frequencies of the arch

Mode	Present study (piezoelectric disks)			Previous study (accelerometers) [15]		
	Experim. (Hz)	FEM (Hz)	Diff. (%)	Experim. (Hz)	FEM* (Hz)	Diff. (%)
1	54.6	52.8	−3.21	50.3	51.9	3.10
2	127.0	127.3	0.25	123.8	124.9	0.81
3	231.1	233.8	1.16	224.7	228.6	1.69
4	360.0	365.1	1.43	359.3	357.6	−0.47
5	521.4	532.1	2.05	509.9	520.7	2.11
6	721.7	718.1	−0.50	716.3	708.1	−1.15

* The masses of the accelerometers were considered in the model

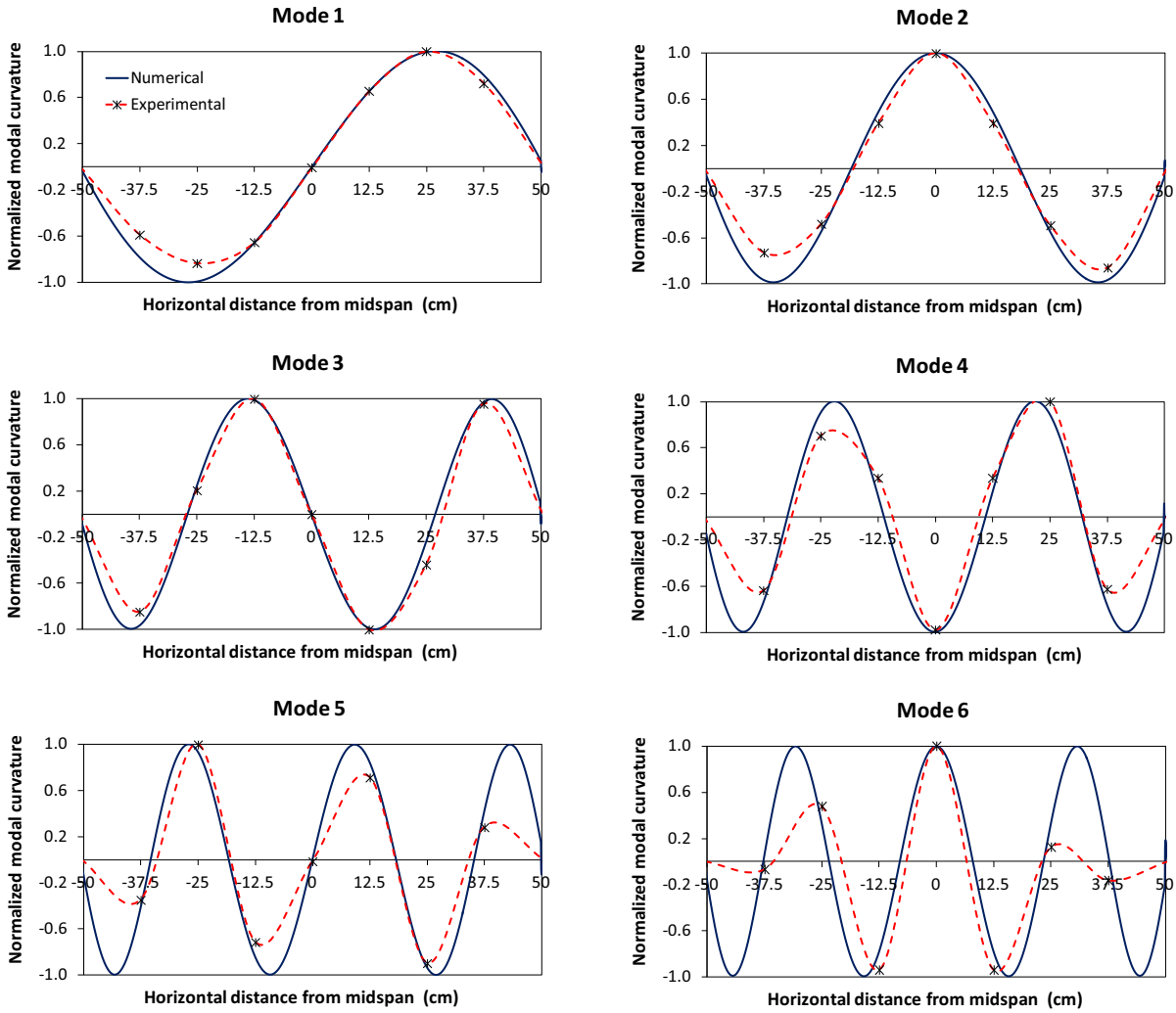

Fig. 8 First six normalized modal curvatures for the parabolic arch in Fig. 7 (present study vs FEM)

Figure 8 shows that the adopted piezoelectric disk could extract the modal curvatures with high precision. Figure 9 shows that the results are good also for the first three mode shapes, but are quite poor for the remaining ones. Lastly, when acceleration vibration signals are considered [15], the first six mode shapes of

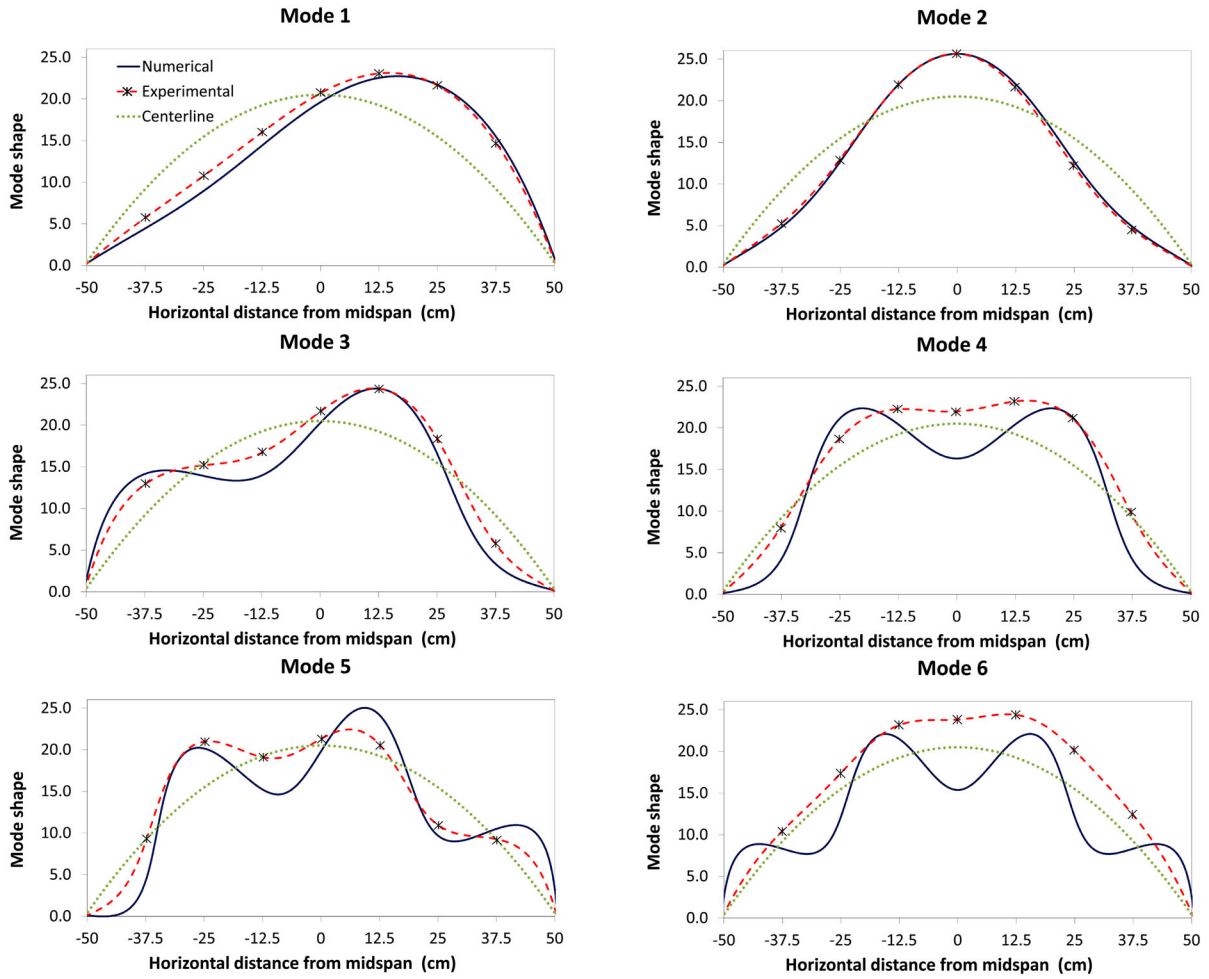

Fig. 9 First six normalized mode shapes for the parabolic arch in Fig. 7 (present study vs FEM)

the parabolic arch are well reproduced, as illustrated by Fig. 10.

We evaluated the correlation among modal curvatures and shapes by *MAC* and *NMD* (see Eqs. (4), (5), respectively). We carried out the correlation analysis considering the lists of curvatures and vertical displacements at the instrumented sections as vectors, for modal curvatures and shapes respectively. Results are in Table 8, and point a very high correlation of experimental and analytical modal curvatures out. The first three mode shapes exhibit good correlation, but this does not occur for the fifth one. In the 4th and 6th modes, shapes were almost completely uncorrelated (bold-face in Table 8), even though the corresponding modal curvatures are very well correlated. As already stated for the cantilever, such a discrepancy shall be due to an error amplification played by the numerical procedure for higher mode shapes (see Fig. 8; the comments provided for the cantilever hold also here). Lastly, Table 8 confirms that when accelerometers are used, the first six experimental and numerical mode shapes of the arch are well correlated. However, limiting the analysis to the first three mode shapes, for which the numerical technique works, the accuracy of piezoelectric transducers is greater than that of accelerometers.

5 Concluding remarks

Piezoelectric disk buzzers were, as long as we know, used in the laboratory for the first time to extract the

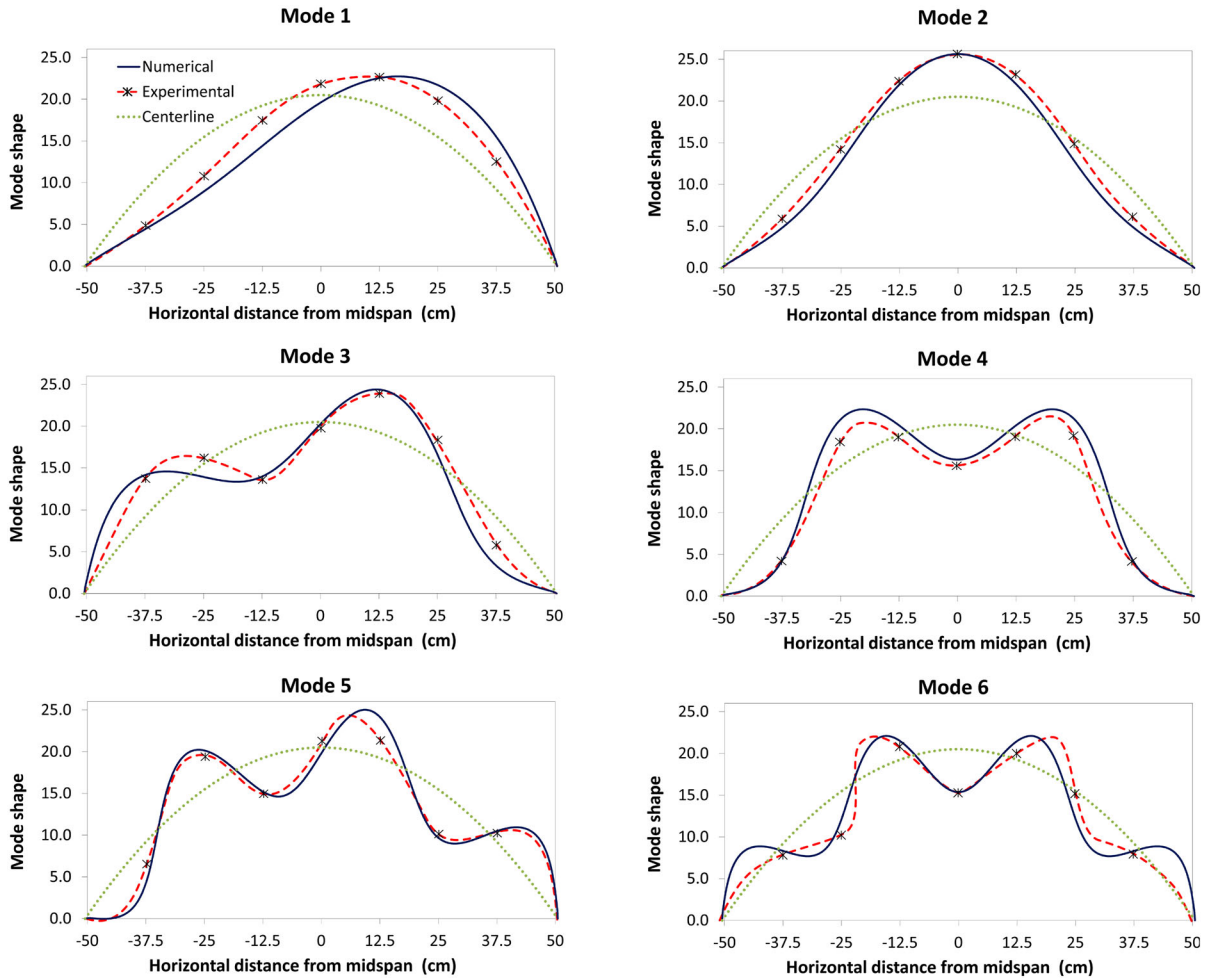

Fig. 10 First six normalized modal curvatures for the arch in Fig. 7 (post-processing of [15] vs FEM)

Table 8 *MAC* and *NMD* values for modal curvatures and mode shapes shown in Figs. 8, 9 and 10

Mode	Modal curvatures		Mode shapes			
	MAC	*NMD*	*MAC*	*NMD*	*MAC*	*NMD*
1	0.9892	0.1044	0.9676	0.1830	0.8610	0.4018
2	0.9894	0.1034	0.9900	0.1003	0.8078	0.4878
3	0.9861	0.1187	0.8429	0.4318	0.8121	0.4810
4	0.9703	0.1748	**0.3513**	**1.3588**	0.9235	0.2878
5	0.9868	0.1158	0.5897	0.8342	0.9568	0.2125
6	0.9461	0.2388	**0.0206**	**6.9000**	0.8598	0.4038
	PZT pickups		Accelerometers			

modal parameters of a cantilever straight beam and a doubly hinged parabolic arch; we already presented such a possibility in a previous work. In this paper, we extended the previous results, and made several comparisons among different experimental setups, with theoretical predictions and other experimental data were made in terms of natural frequencies, modal curvatures, and mode shapes. Results indicate that the adopted piezoelectric disk proved to be an efficient tool for detecting natural frequencies and modal curvatures and shapes of metallic specimens, at least at the laboratory scale, for both straight and curved elements. We shall remark, however, that a reliable estimation of mode shapes requires limiting the evaluation to just the first few modes or increasing the number of sensors, due to the error amplification played by the interpolation-integration numerical technique. The voltage signal generated by piezoelectric disks during vibration is proportional to the

specimen surface deformation (average strain over the contact area): thus, privileged placements of such sensors are the regions where strains, not displacements, are higher. In this sense, our application is pretty close to SMT, even though a measure of the effective strain cannot be probably obtained via piezoelectric disk buzzers, at least without any calibration; this problem was not addressed by this study. These sensors could anyway be suitable, for instance, in damage identification based on modal testing, where modal curvature is one of primary parameters [29]. The advantages stated in the abstract and the results presented here make the authors believe that further investigations on the effectiveness of piezoelectric disks for experimental modal analysis would be of interest. Their response on non-metallic specimens (e.g., concrete, masonry), plus their application on full-scale structures, should be assessed. Moreover, their capability of extracting modal damping from measured signals should also be analyzed.

Acknowledgments We gratefully acknowledge the support of institutional grants of the University "La Sapienza", Rome. Special thanks also to Eng. M. Tonici for the needful cooperation provided in many phases of this study.

References

1. De Silva CW (2000) Vibration. CRC Press, Boca Raton, Fundamentals and Practice
2. Ewins DJ (2000) Modal testing: theory, practice and application, 2nd edn. Research Studies Press, Baldock
3. Fu Z-F, He J (2001) Modal Analysis. Butterworth-Heinemann, Oxford
4. Hillary B, Ewinns DJ (1984) The use of strain gauges in force determination and frequency response function measurement, In: Proceedings of the 2nd IMAC, pp 627–634
5. YI S, Kong FR, Chang YS (1984) Vibration modal analysis by means of impulse excitation and measurement using strain gauges, In: Proceedings of the IMechE C308/84, pp 391–396
6. Stacker C (1985) Modal analysis efficiency improved via strain frequency response functions, In: Proceedings of the 3rd IMAC, pp 612–617
7. Song T, Zhang PQ, Feng WQ, Huang TC (1986) The application of the time domain method in strain modal analysis, In: Proceedings of the 4th IMAC, pp 31–37
8. Debao L, Hongcheng Z, Bo W (1989) The principle and techniques of experimental strain modal analysis, In: Proceedings of the 7th IMAC, pp 1285–1289
9. Bernasconi O, Ewins DJ (1989) Application of strain modal testing to real structures, Proceedings of the 7th IMAC, pp 1453–1464
10. Bernasconi O, Ewins DJ (1989) Modal strain/stress fields. Int J Anal Exp Modal Anal 4(2):68–79
11. Yam LH, Leung TP, Li DB, Xue KZ (1996) Theoretical and experimental study of modal strain analysis. J Sound Vib 191(2):251–260
12. Rovšček D, Slavič J, Boltežar M (2013) The use of strain sensors in an experimental modal analysis of small and light structures with free-free boundary conditions. J Vib Control 19(7):1072–1079
13. Kranjc T, Slavič J, Boltežar M (2013) The mass normalization of the displacement and strain mode shapes in a strain experimental modal analysis using the mass-change strategy. J Sound Vib 332:6968–6981
14. Mucchi E, Dalpiaz G, (2014) On the use of piezoelectric strain sensors for experimental modal analysis. In: Menghetti U, Maggiore A, Parenti Castelli V (eds) Settima giornata di studio Ettore Funaioli, 19 luglio 2013. Quaderni del DIEM—GMA—Atti di giornate di studio vol 7, Società Editrice Esculapio, Bologna, pp 293–301 (http://amsacta.unibo.it/4064/)
15. Lofrano E, Paolone A, Romeo F, (2014) Damage identification in a parabolic arch through the combined use of modal properties and empirical mode decomposition. In: Proceedings of the 9th international conference on structural dynamics, EURODYN 2014, Porto, Portugal, 30 June–2 July 2014
16. Romeo F, Lofrano E, Paolone A (2014) Damage identification in a parabolic arch via orthogonal empirical mode decomposition, In: Proceedings of the ASME (IDETC/CIE/VIB) international conference, ASME 2014, Buffalo, USA, 17–20 August 2014
17. Piana G, Brunetti M, Carpinteri A, Malvano R, Manuello A, Paolone A (2016) On the use of Piezo-electric sensors for experimental modal analysis. In: Song et al. (eds) Dynamic behavior of materials, volume 1. In: Proceedings of the 2015 annual conference on experimental and applied mechanics, Springer, 2016
18. Galef AE (1968) Bending frequencies of compressed beams. J Acoust Soc Am 44(8):643
19. Bokaian A (1988) Natural frequencies of beams under compressive axial loads. J Sound Vib 126(1):49–65
20. Bokaian A (1990) Natural frequencies of beams under tensile axial loads. J Sound Vib 142(3):481–498
21. Clough RW, Penzien J (1975) Dynamics of structures. McGraw-Hill, New York
22. Virgin NL (2007) Vibration of axially loaded structures. Cambridge University Press, New York
23. Bažant ZP, Cedolin L (1991) Stability of structures. Oxford University Press, Oxford
24. Blevins RD (1979) Formulas for natural frequencies and mode shapes. Van Nostrand Rheinhold, New York
25. Chapra SC, Canale RP (2010) Numerical methods for engineers, 6th edn. McGraw-Hill, New York
26. Allemang RJ, Brown DL, (1982) A Correlation coefficient for modal vector analysis,In: Proceedings of the 1st IMAC, Orlando, Florida, 1982
27. Maya NMM, Silva JMM (eds) (1997) Theoretical and experimental modal analysis. Research Studies Press, Taunton
28. Pau A, Greco A, Vestroni F (2011) Numerical and experimental detection of concentrated damage in a parabolic arch by measured frequency variations. J Vib Control 17(4):605–614
29. Dessi D, Camerlengo G (2015) Damage identification techniques via modal curvature analysis: overview and comparison. Mech Syst Signal Process 52–53:181–205